

Generalized Hamiltonian for Kekulé graphene and the emergence of valley-cooperative Klein tunneling

Santiago Galván y García,^{1,*} Thomas Stegmann,^{1,†} and Yonatan Betancur-Ocampo^{1,‡}

¹*Instituto de Ciencias Físicas, Universidad Nacional Autónoma de México, Cuernavaca 62210, México*

We introduce a generalized Hamiltonian describing not only all topological phases observed experimentally in Kekulé graphene (KekGr) but predicting also new ones. These phases show features like a quadratic band crossing point, valley splitting, or the crossing of conduction bands, typically induced by Rashba spin-orbit interactions or Zeeman fields. The electrons in KekGr behave as Dirac fermions and follow pseudo-relativistic dispersion relations with Fermi velocities, rest masses, and valley-dependent self-gating. Transitions between the topological phases can be induced by tuning these parameters. The model is applied to study the current flow in KekGr *pn* junctions evidencing a novel cooperative transport phenomenon, where Klein tunneling goes along with a valley flip. These junctions act as perfect filters and polarizers of massive Dirac fermions, which are the essential devices for valleytronics. The plethora of different topological phases in KekGr may also help to establish phenomena from spintronics.

Over the last two decades, graphene has attracted the scientific community due to its outstanding properties [1]. One of them is the fact that the electrons in graphene present, apart from the intrinsic spin, two pseudospins: the sublattice and the valley pseudospin [2, 3]. The latter one may be used for a new type of electronics called valleytronics [4–7]. In order to fabricate valleytronic devices, it has been shown that the valley pseudospin can be manipulated by strain and defects [4, 6, 8–14]. Another strategy for valleytronics is to break the chiral symmetry in graphene through a Kekulé distortion [15–19]. This distortion consists of alternating hopping parameters and on-site energies, leading to an enlarged unit cell of six atoms [16–18, 20–31]. Currently, two topological phases in Kekulé graphene (KekGr) have been predicted and confirmed experimentally [15, 17, 19, 32]. Moreover, KekGr may establish a bridge between valleytronics and spintronics to realize intriguing phenomena predicted in semiconductors [3, 33–40]. Note that the chiral symmetry breaking observed in KekGr is also of crucial importance to emulate mass generation of elementary particles in condensed matter, as studied in the standard model [41, 42].

Recently, Kekulé distortions were generated by intercalating Li atoms between a graphene sheet and a SiC substrate [19, 32], confirming the chiral symmetry breaking predicted by effective models based on a tight-binding approach [30, 43]. Nevertheless, the current models do not explain some topological phases recently discovered in experimental studies of KekGr [19]. Here, we propose a generalized Hamiltonian that embodies all the known results in KekGr and predicts various new topological phases. This generalized Hamiltonian is used to study the transport properties of KekGr *pn* junctions. We observe a valley-flip process due to the valley-dependent Fermi velocity, giving rise to a novel Klein tunneling. This effect is persistent against variations of the Fermi level and electrostatic gating, and emerges in all topological phases of KekGr within the ultra-pseudo-relativistic

limit. Moreover, the proposed devices fully valley polarize the current flow (in certain parameter regime) and hence, are of relevance for valleytronic applications.

KekGr shows bond distortions of Y and O shape, known as Kek-Y and Kek-O textures. This rearrangement in the lattice causes drastic changes in the electronic band structure. The Dirac cones in the valleys K^+ and K^- are folded towards the Γ point in the Brillouin zone [18, 21, 26, 27, 30]. In the case of the Kek-O texture, the low-energy regime shows degenerated energy bands separated by a gap, while in the case of the Kek-Y, the low-energy excitations follow a non-degenerated and valley-dependent linear dispersion relation [15]. The tuning of the onsite energies of specific atoms in the unit cell breaks the chiral symmetry for obtaining simultaneously massless and massive Dirac fermions. Here, we propose the most general effective Hamiltonian of KekGr

$$H_{\text{KekGr}} = \begin{pmatrix} 2\lambda & v_\sigma p_- & v_\tau p_- & 2\eta \frac{p_-}{p_+} \\ v_\sigma p_+ & 2\rho & 2\delta & v_\tau p_- \\ v_\tau p_+ & 2\delta & 2\rho & v_\sigma p_- \\ 2\eta \frac{p_+}{p_-} & v_\tau p_+ & v_\sigma p_+ & 2\lambda \end{pmatrix} \quad (1)$$

to describe the superposition of two different massive Dirac fermions in the two valleys. In the Hamiltonian (1), v_σ is the Fermi velocity of pristine graphene, v_τ is the velocity that quantifies the magnitude of the Kekulé distortion, and $\mathbf{p} = (p_x, p_y)$ is the linear momentum with $p_\pm = p_x \pm ip_y$. The parameters λ , ρ , and δ are related with the onsite potential and break the chiral symmetry for one or both valleys, while the parameter η quantifies the spin-orbit interaction. The eigenenergies of the Hamiltonian (1) are

$$E_s^\nu = \xi_\nu + s\sqrt{(v_\sigma + \nu v_\tau)^2 p^2 + \mu_\nu^2}, \quad (2)$$

where $s = \text{sign}(E - \xi_\nu)$ and $\nu = \pm 1$ are the band and valley index, respectively. The self-gating and rest energies ξ_ν and μ_ν depend on the parameters of the Hamiltonian (1) as $\xi_\nu = \lambda + \rho + \nu(\delta + \eta)$ and $\mu_\nu = -\delta + \eta + \nu(\lambda - \rho)$,

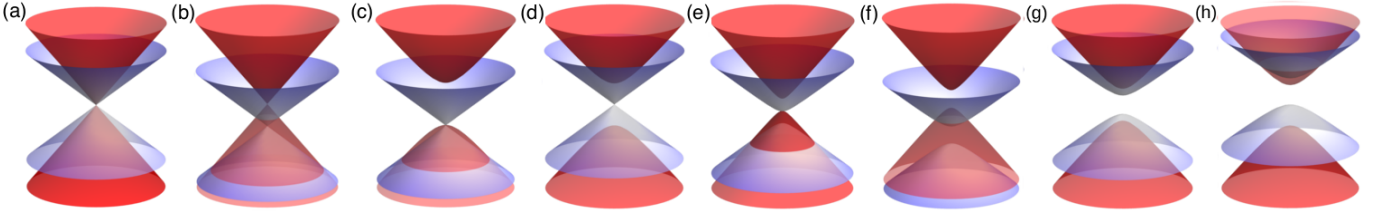


Figure 1. Topological phases of Kekulé graphene (KekGr). (a) and (b) Massless Dirac fermions in both valleys. (c) and (d) Chiral symmetry breaking in a single valley, where electrons behave as massless and massive Dirac fermions. (e) and (f) Quadratic band crossing point and valley-orbit coupling, respectively. (g) Zeeman-like effect. (h) Crossing of conduction bands.

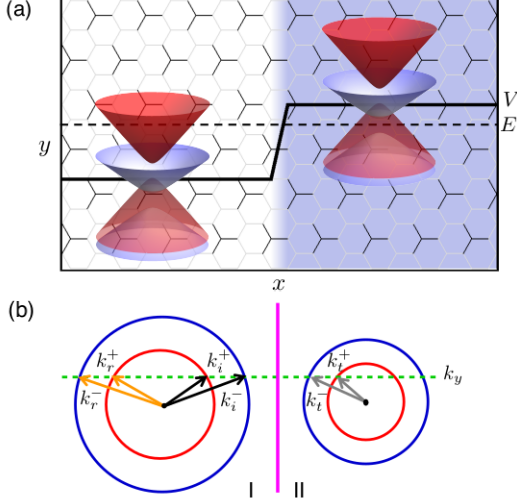


Figure 2. KekGr pn junction. (a) Potential profile of the pn junction showing the shift of the bandstructure in the two regions. (b) Kinematical construction that shows the conservation of energy E , momentum k_y , and current density. The arrows represent the wave vectors \mathbf{k}^ν for the states involved in the scattering process.

respectively. Tuning these parameters leads to different phases, which can be obtained in KekGr modulating the onsite energies, hopping parameters, and spin-orbit coupling, as shown in tight-binding calculations [18]. In general, electrons in KekGr behave like a mixture of massive Dirac fermions with relatively shifted dispersion relations identical to relativistic particles having limit velocities $v_\sigma + \nu v_\tau$. In Fig. 1, we show a gallery of topological phases such as massless Dirac fermions in both valleys, chiral symmetry breaking in a single valley, quadratic band crossing point, field-free Zeeman-like effect, and valley-orbit coupling. Atypical phases are obtained, for instance, the crossing of the conduction bands of the two valleys.

To study the electronic transport of KekGr in the multiple possible phases displayed in Fig. 1, we make a plane wave ansatz using the eigenstates of the Hamiltonian (1)

$$\Psi_s^\nu(\mathbf{k}, \mathbf{r}) = \mathbf{u}_s^\nu(\mathbf{k}) e^{i\mathbf{k} \cdot \mathbf{r}} \quad (3)$$

where

$$\mathbf{u}_s^\nu(\mathbf{k}) = \frac{(1, \alpha_s^\nu e^{i\phi(\mathbf{k})}, \nu \alpha_s^\nu e^{i\phi(\mathbf{k})}, \nu e^{2i\phi(\mathbf{k})})}{\sqrt{2[1 + (\alpha_s^\nu)^2]}}, \quad (4)$$

$$\alpha_s^\nu = \frac{E_s^\nu - \xi_\nu - \nu \mu_\nu}{\sqrt{(E_s^\nu - \xi_\nu)^2 - \mu_\nu^2}}, \quad \phi(\mathbf{k}) = \arctan\left(\frac{k_y}{k_x}\right). \quad (5)$$

The linear momentum \mathbf{p} has the eigenvalue $p = \hbar k$ and $\mathbf{u}_s^\nu(\mathbf{k})$ are the four spinors of the Hamiltonian (1). The pseudospin angle is $\phi(\mathbf{k})$ and α_s^ν is the generalization of the band index s of massless Dirac fermions.

We consider a KekGr pn junction where the electrons, injected at energy E , impinge an electrostatic potential V , see Fig. 2(a). The electrons are injected as a superposition of states from both valleys

$$\mathbf{w}_s(\mathbf{r}) = \sum_\nu a^\nu \mathbf{u}_s^\nu(\mathbf{k}_i^\nu) e^{i\mathbf{k}_i^\nu \cdot \mathbf{r}}, \quad (6)$$

where $\mathbf{k}_i^\nu = (k_{i,x}^\nu, k_y)$ is the incident wave vector. The component k_y is the conserved linear momentum along the interface, which is parametrized in terms of the incidence angle θ of electrons in the valley K^+

$$k_y = \frac{\sqrt{(E - \xi_+)^2 - \mu_+^2}}{\hbar(v_\sigma + v_\tau)} \sin \theta. \quad (7)$$

The amplitudes a^ν indicate the probability weight for the valley K^ν . For instance, $a^+ = 1$ and $a^- = 0$ correspond to a full polarization of the injected electrons in the valley K^+ . These electrons impinge the interface with different incidence angles because the component k_x depends on the valleys, as shown in Fig. 2(b). Therefore, the wave function in region I is

$$\Psi^I(\mathbf{r}) = \mathbf{w}_s(\mathbf{r}) + \sum_\nu \mathbf{u}_s^\nu(\mathbf{k}_r^\nu) r^\nu e^{i\mathbf{k}_r^\nu \cdot \mathbf{r}}, \quad (8)$$

where $\mathbf{k}_r^\nu = (k_{r,x}^\nu, k_y)$ are the wave vectors of the reflected electrons and r^ν are the reflected amplitudes. In region II of the pn junction, where the electrostatic potential shifts the dispersion relation, we have the wavefunction

$$\Psi^{II}(\mathbf{r}) = \sum_\nu t^\nu \mathbf{u}_s^\nu(\mathbf{k}_t^\nu) e^{i\mathbf{k}_t^\nu \cdot \mathbf{r}}, \quad (9)$$

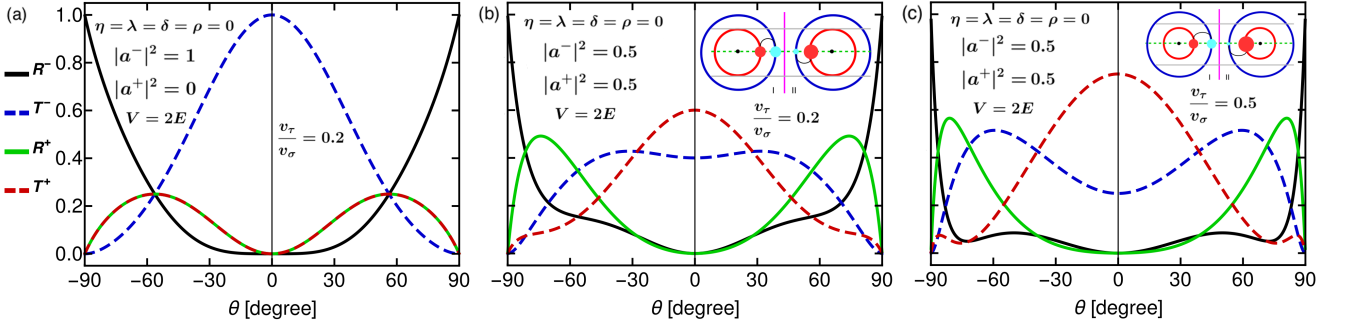


Figure 3. (a)-(c) Reflection and transmission probabilities as a function of the incidence angle for different Kekulé distortions and valley polarizations of the injected electrons. The insets in (b) and (c) show the kinematical construction to illustrate the valley-cooperative Klein tunneling. The incident and transmitted electrons are represented by the superposition of electronic states in the valleys K^ν , where the size of the circles indicates the occupation of the valleys.

with the band index $s' = \text{sign}(E - \xi_\nu - V)$. The transmitted wave vectors and amplitudes are $\mathbf{k}_t^\nu = (k_{t,x}^\nu, k_y^\nu)$ and t^ν , respectively. The continuity of the wave function $\Psi^I(\mathbf{k}, \mathbf{r})$ and $\Psi^{II}(\mathbf{k}, \mathbf{r})$ at the interface of the pn junction allows determining the reflection and transmission coefficients

$$R^\nu = -\frac{J_{s,x}^\nu(\mathbf{k}_r^\nu)}{\sum_\nu |a^\nu|^2 J_{s,x}(\mathbf{k}_i^\nu)} |r^\nu|^2, \quad (10)$$

$$T^\nu = \frac{J_{s',x}^\nu(\mathbf{k}_t^\nu)}{\sum_\nu |a^\nu|^2 J_{s,x}(\mathbf{k}_i^\nu)} |t^\nu|^2, \quad (11)$$

with the probability current density

$$J_{s,x}^\nu(\mathbf{k}) = \frac{\partial E_s^\nu}{\partial p_x} = \frac{2\alpha_s^\nu(v_\sigma + \nu v_\tau)}{1 + (\alpha_s^\nu)^2} \cos \phi(\mathbf{k}). \quad (12)$$

The reflection and transmission coefficients satisfy $\sum_\nu (R^\nu + T^\nu) = 1$ due to the conservation of J_x .

We analyze the case of massless Dirac fermions with $\mu_\nu = 0$ in the valleys K^- and K^+ . Figure 3(a) shows the behavior for the reflection and transmission coefficients when the incident state is fully polarized in the valley K^- . For normal incidence, perfect tunneling appears due to the conservation of the pseudospin, while electrons with incidence angles $\theta \neq 0^\circ$ have non-zero probabilities for the reflection and transmission in both valleys. The situation is identical if we inject electrons polarized in the valley K^+ . A counter-intuitive transmission phenomenon occurs when the normally incident electrons occupy both valleys, $|a^\nu|^2 = 0.5$. In this case backscattering is absent ($R^\nu = 0$) but contrary to the expectation of finding an transmitted current that is distributed equally in both valleys, we obtain electron currents in the fractions 0.6 and 0.4 for the valleys K^- and K^+ , respectively, as shown in Fig. 3(b). 10% of the electrons in valley K^- make a valley-flip to cross *cooperatively* the interface without backscattering. We name this unusual and novel transport phenomenon *valley-cooperative Klein tunneling*, as sketched in the insets of Fig. 3(b).

The valley flip process is controlled only by the Kekulé distortion. Increasing the velocity v_τ , the difference of $T_+ - T_-$ under normal incidence also increases, as shown in Fig. 3(c). This novel effect is due to the Kekulé distortion and the conservation of the pseudospin. It is independent of the Fermi level and the electrostatic potential, see Fig. 4(a). To understand the valley-cooperative Klein tunneling, we calculate the transmission probabilities for normal incidence and weights a^\pm

$$T^\pm(0) = \frac{(v_\sigma \pm v_\tau)|a^\pm|^2}{\sum_\nu (v_\sigma + \nu v_\tau)|a^\nu|^2}, \quad (13)$$

where the pseudospin angles are $\phi_i^- = \phi_i^+ = 0$, $\phi_r^- = \phi_r^+ = \pi$, and $\phi_t^- = \phi_t^+ = (s - s')\pi/2$. For the reflection coefficients, we have $R^\pm = 0$. For $|a^\nu|^2 = 0.5$ the Eq. (13) can be simplified to $T^\pm(0) = \frac{1}{2}(1 \pm \frac{v_\tau}{v_\sigma})$. Clearly, we observe that $T^-(0) + T^+(0) = 1$. We recover the conventional Klein tunneling in graphene making $v_\tau = 0$, and as expected, unpolarized current under normal incidence crosses perfectly the electrostatic potential [44, 45]. The extreme case $v_\sigma = v_\tau$ indicates that all the electrons in the valley K^- perform a valley-flip to cross perfectly the junction, resulting in a fully valley polarized current. Moreover, $v_\sigma = v_\tau$ merges the conduction and valence bands in the valley K^- to a flat band, giving rise to super-Klein tunneling, which is a typical phenomenon in the scattering of pseudospin-one particles [46–55].

We analyze the tunneling as a function of the electron energy E under normal incidence for situations with chiral symmetry breaking, as shown in Fig. 4(b) to (f). We set the weights $|a^\nu|^2 = 0.5$ in the injected state. Despite a gap opening in the valley K^+ , the distinctive signature of massless Dirac fermions persists due to the absence of backscattering in the valley K^- for all energies, see Fig. 4(b). However, the fraction of massless Dirac fermions in the valley K^- crossing the interface is less than the initial quantity $|a^-|^2 = 0.5$. As expected, the reflection probability of massive Dirac fermions is nonzero, but the sum $R^+ + T^+ > 0.5$. Part of the current

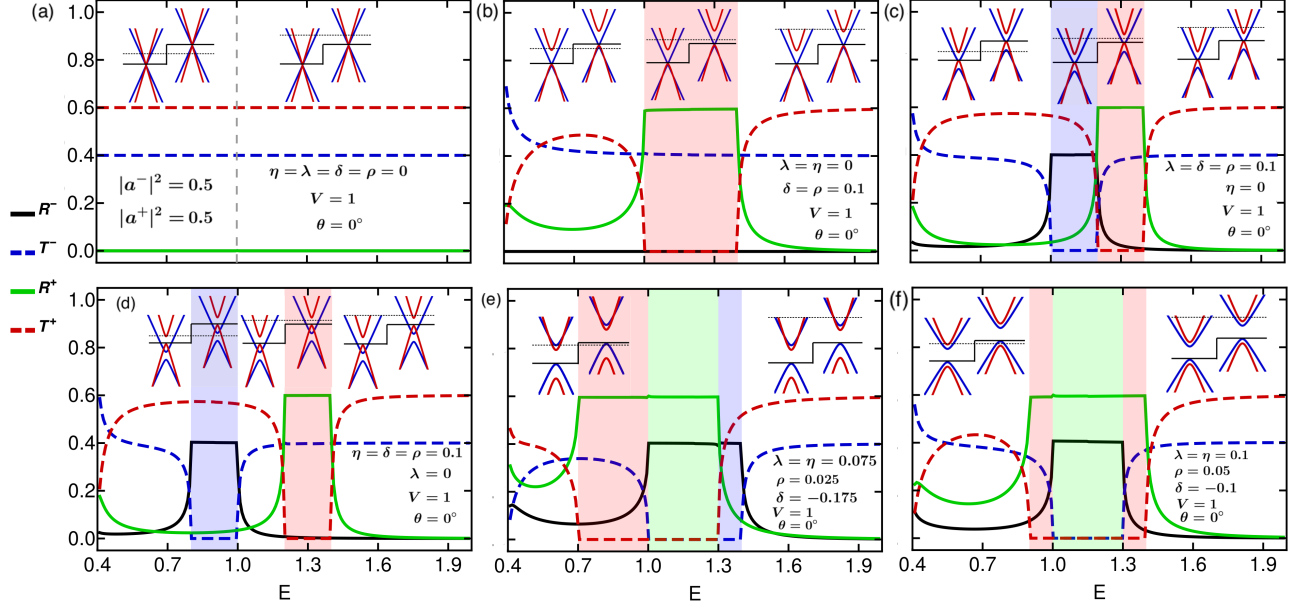


Figure 4. Reflection and transmission probabilities as a function of the Fermi energy E under normal incidence for different KekGr pn junctions. (a) Massless Dirac fermions in both valleys, the dashed gray line separates the interband ($E < 1$) and intraband ($E > 1$) tunneling regime. (b) Chiral symmetry breaking in a single valley, (c) quadratic band crossing point, (d) valley-orbit coupling, (e) crossing conduction bands, and (f) Zeeman-like effect. The insets show the band structure of the junction, indicating E by a dotted line. The red and blue rectangles represent the regions of perfect valley filtering. The green regions indicate the transport gap.

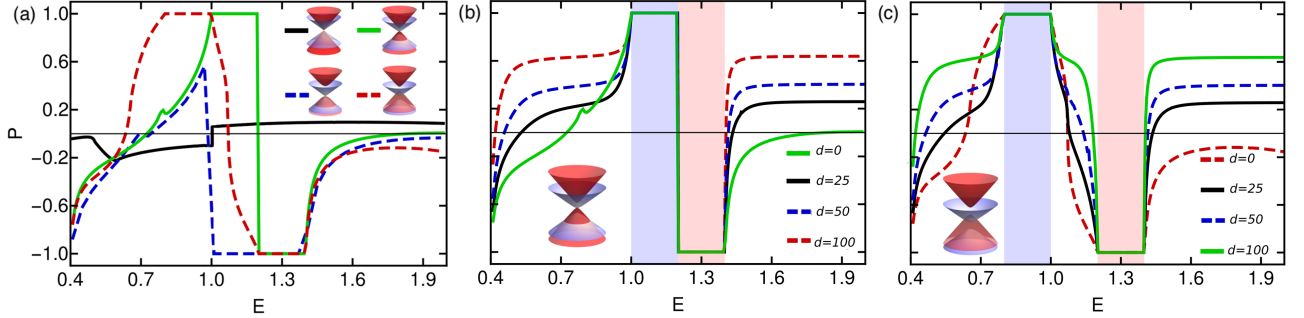


Figure 5. Polarization as a function of the Fermi energy E for the cases of massless Dirac fermions in both valleys, chiral symmetry breaking in a single valley, quadratic band crossing point, and valley-orbit coupling in (a). The effect of the smoothness of the junction for the cases of a quadratic band crossing point and valley-orbit coupling in (b) and (c), respectively.

flow of massless Dirac fermions converts to massive particles. The fraction of electrons realizing the valley flip and obtaining a non-zero mass is equal to $v_\tau/v_\sigma = 0.1$ independently of the Fermi level. By increasing the energy, massive Dirac fermions are filtered totally in the intraband transmission regime due to the absence of the electronic band for the valley K^+ . In this energy range, the junction works as a perfect valley filter, see the red shaded region. In the pseudo-ultra-relativistic limit (i.e. at high energies), the reflection and transmission probabilities have an identical behavior compared with the previously discussed gapless case. The reflection and transmissions probabilities are constant for normal incidence

and independent of the energy due to the conservation of the pseudospin.

The valley-flip process persists even if the chiral symmetry is broken in both valleys, as shown in Fig. 4(c) to (f). The transmission probabilities for the two valleys have the values of 0.6 and 0.4 in the pseudo-ultra-relativistic limit, because the valley-flip process depends only on the Fermi velocities $v_\sigma + \nu v_\tau$ but not on the self-gating potentials ξ_ν and rest energies μ_ν . However, the tuning of these parameters can be used to design junctions acting as a valley switch. Depending on the Fermi energy, electrons from a certain valley are filtered, see the blue and red shaded regions in Fig. 4(c)-(f). For some

topological phase these regions can be separated by a transport gap, see the green shaded region in Fig. 4(e) and (f).

To quantify the degree of polarization P in KekGr pn junctions, we define

$$P = \frac{\langle T^+ \rangle - \langle T^- \rangle}{\langle T^+ \rangle + \langle T^- \rangle}, \quad (14)$$

where $\langle T^\nu \rangle$ is the angular averaged transmission of Eq. (11). Figure 5(a) shows the polarization in junctions for the topological phases of Fig. 1(a), (c), (e), and (f). We can see that the partial polarization of massless Dirac fermions (black curve) remains almost constant for the intraband transmission ($E > V$) and has the approximated value of $P \approx v_\tau/v_\sigma = 0.1$. Note that this asymptotic value of P is unaffected by the smoothness of the junction, being a signature of the valley-flip process that may be detected experimentally. However, the valley polarization of massless Dirac fermions is rather low. A fully valley polarized current flow is achieved by breaking the chiral symmetry. Moreover, the sign of the polarization can be changed by tuning the Fermi energy within the different gaps of the valleys, making these systems a perfect valley switch. Note that the transition is abrupt in the case of a quadratic band crossing point (green curve), but smooth in the case of valley orbit coupling (red dashed curve).

To investigate the robustness of our findings, we consider a smooth electrostatic potential changing linearly over the distance $2d$ [45, 56]. In this case the electrons have to tunnel through a forbidden region, which reduces the transmission probability exponentially. However, the polarization of the current flow is unaffected, as shown in Fig. 5(b) and (c). The asymptotic value of P at higher energies increases due to the collimation effect. Electrons cross preferentially under normal incidence because the forbidden region grows for grazing incidence [57–59]. However, this goes along with an increase of the reflections reducing the overall efficiency of the device.

In summary, the particular design of Kekulé textures in graphene leads to atypical transport phenomena such as valley-cooperative Klein tunneling and valley polarization of currents. We proposed a generalized Hamiltonian in Eq. (1) that embodied multiple topological phases with electronic band structures identical to systems with Rashba spin-orbit interactions. We also reported new topological phases such as a Zeeman effect without magnetic field and crossing of conduction bands through the tuning of the effective parameters of the Hamiltonian (1), as shown in Fig. 1. In Kekulé graphene pn junctions, the chiral symmetry breaking serves as a mechanism to give mass to Dirac fermions through a valley-flip process, similar to the Higgs boson of elementary particles in the standard model. Moreover, these devices can be used to filter perfectly massive Dirac fermions, as seen in

Fig. 4 (a) to (c), and obtain fully valley polarized currents, which is the essential building block for valleytronics. Additionally, we showed that the smoothness of the junction does not affect the total polarization and the signal of valley-cooperative tunneling, making it feasible for experimental realizations.

SGyG acknowledges a scholarship from CONACYT. We acknowledge financial support from CONACYT Project A1-S-13469 and the UNAM-PAPIIT research grant IA103020.

* santiagogyg@icf.unam.mx

† stegmann@icf.unam.mx

‡ ybetancur@icf.unam.mx

- [1] K. S. Novoselov, A. K. Geim, S. V. Morozov, D. Jiang, M. I. Katsnelson, I. V. Grigorieva, S. V. Dubonos, and A. A. Firsov, Two-dimensional gas of massless Dirac fermions in graphene, *Nature* **438**, 197 (2005).
- [2] A. H. C. Neto, F. Guinea, N. M. R. Peres, K. S. Novoselov, and A. K. Geim, The electronic properties of graphene, *Rev. Mod. Phys.* **81**, 109 (2009).
- [3] D. Bercioux and P. Lucignano, Quantum transport in Rashba spin-orbit materials: a review, *Rep. Prog. Phys.* **78**, 106001 (2015).
- [4] A. Rycerz, J. Tworzydło, and C. W. J. Beenakker, Valley filter and valley valve in graphene, *Nat. Phys.* **3**, 172 (2007).
- [5] J. R. Schaibley, H. Yu, G. Clark, P. Rivera, J. S. Ross, K. L. Seyler, W. Yao, and X. Xu, Valleytronics in 2D materials, *Nat. Rev. Mater.* **1**, 16055 (2016).
- [6] D. Gunlycke and C. T. White, Graphene Valley Filter Using a Line Defect, *Phys. Rev. Lett.* **106**, 136806 (2011).
- [7] M. Hossain, M. Ma, K. Villegas-Rosales, Y. Chung, L. Pfeiffer, K. West, K. Baldwin, and M. Shayegan, Spontaneous Valley Polarization of Itinerant Electrons, *Phys. Rev. Lett.* **127**, 116601 (2021).
- [8] T. Stegmann and N. Szpak, Current flow paths in deformed graphene: from quantum transport to classical trajectories in curved space, *New J. Phys.* **18**, 053016 (2016).
- [9] T. Stegmann and N. Szpak, Current splitting and valley polarization in elastically deformed graphene, *2D Mater.* **6**, 015024 (2018).
- [10] T. Low and F. Guinea, Strain-Induced Pseudomagnetic Field for Novel Graphene Electronics, *Nano Lett.* **10**, 3551 (2010).
- [11] X. W. Zhao, Y. Li, R. D. Liang, G. C. Hu, X. B. Yuan, and J. F. Ren, Enhanced valley polarization at valence/conduction band in transition-metal-doped WTe₂ under strain force, *Appl. Surf. Sci.* **504**, 144367 (2020).
- [12] T. Fujita, M. B. A. Jalil, and S. G. Tan, Valley filter in strain engineered graphene, *Appl. Phys. Lett.* **97**, 043508 (2010).
- [13] J. L. Garcia-Pomar, A. Cortijo, and M. Nieto-Vesperinas, Fully Valley-Polarized Electron Beams in Graphene, *Phys. Rev. Lett.* **100**, 236801 (2008).
- [14] D. Zhong, K. L. Seyler, X. Linpeng, R. Cheng, N. Sivadas, B. Huang, E. Schmidgall, T. Taniguchi, K. Watanabe, M. A. McGuire, et al., Van der Waals engi-

- neering of ferromagnetic semiconductor heterostructures for spin and valleytronics, *Sci. Adv.* **3**, e1603113 (2017).
- [15] C. Gutiérrez, C.-J. Kim, L. Brown, T. Schiros, D. Nordlund, E. B. Lochocki, K. M. Shen, J. Park, and A. N. Paspas, Imaging chiral symmetry breaking from Kekulé bond order in graphene, *Nat. Phys.* **12**, 950 (2016).
- [16] Y. Liu, C.-S. Lian, Y. Li, Y. Xu, and W. Duan, Pseudospins and Topological Effects of Phonons in a Kekulé Lattice, *Phys. Rev. Lett.* **119**, 255901 (2017).
- [17] D. Eom and J.-Y. Koo, Direct measurement of strain-driven Kekulé distortion in graphene and its electronic properties, *Nanoscale* **12**, 19604 (2020).
- [18] G. Giovannetti, M. Capone, J. van den Brink, and C. Ortix, Kekulé textures, pseudospin-one Dirac cones, and quadratic band crossings in a graphene-hexagonal indium chalcogenide bilayer, *Phys. Rev. B* **91**, 121417 (2015).
- [19] C. Bao, H. Zhang, T. Zhang, X. Wu, L. Luo, S. Zhou, Q. Li, Y. Hou, W. Yao, L. Liu, et al., Experimental Evidence of Chiral Symmetry Breaking in Kekulé-Ordered Graphene, *Phys. Rev. Lett.* **126**, 206804 (2021).
- [20] C. Chamon, Solitons in carbon nanotubes, *Phys. Rev. B* **62**, 2806 (2000).
- [21] S. Konschuh, M. Gmitra, and J. Fabian, Tight-binding theory of the spin-orbit coupling in graphene, *Phys. Rev. B* **82**, 245412 (2010).
- [22] C.-Y. Hou, C. Chamon, and C. Mudry, Electron Fractionalization in Two-Dimensional Graphenelike Structures, *Phys. Rev. Lett.* **98**, 186809 (2007).
- [23] L.-H. Wu and X. Hu, Topological Properties of Electrons in Honeycomb Lattice with Detuned Hopping Energy, *Sci. Rep.* **6**, 1 (2016).
- [24] A. Pachoud, A. Ferreira, B. Özyilmaz, and A. H. C. Neto, Scattering theory of spin-orbit active adatoms on graphene, *Phys. Rev. B* **90**, 035444 (2014).
- [25] Y. Ren, X. Deng, Z. Qiao, C. Li, J. Jung, C. Zeng, Z. Zhang, and Q. Niu, Single-valley engineering in graphene superlattices, *Phys. Rev. B* **91**, 245415 (2015).
- [26] J. W. F. Venderbos, M. Manzardo, D. V. Efremov, J. van den Brink, and C. Ortix, Engineering interaction-induced topological insulators in a $\sqrt{3} \times \sqrt{3}$ substrate-induced honeycomb superlattice, *Phys. Rev. B* **93**, 045428 (2016).
- [27] E. Andrade, R. Carrillo-Bastos, and G. G. Naumis, Valley engineering by strain in Kekulé-distorted graphene, *Phys. Rev. B* **99**, 035411 (2019).
- [28] J. J. Wang, S. Liu, J. Wang, and J.-F. Liu, Valley-coupled transport in graphene with Y-shaped Kekulé structure, *Phys. Rev. B* **98**, 195436 (2018).
- [29] J. J. Wang, S. Liu, J. Wang, and J.-F. Liu, Valley supercurrent in the Kekulé graphene superlattice heterojunction, *Phys. Rev. B* **101**, 245428 (2020).
- [30] O. V. Gamayun, V. P. Ostroukh, N. V. Gnezdilov, I. Adagideli, and C. W. J. Beenakker, Valley-momentum locking in a graphene superlattice with Y-shaped Kekulé bond texture, *New J. Phys.* **20**, 023016 (2018).
- [31] M. A. Mojarro, V. G. Ibarra-Sierra, J. C. Sandoval-Santana, R. Carrillo-Bastos, and G. G. Naumis, Dynamical Floquet spectrum of Kekulé-distorted graphene under normal incidence of electromagnetic radiation, *Phys. Rev. B* **102**, 165301 (2020).
- [32] C. Virojanadara, S. Watcharinyanon, A. A. Zakharov, and L. I. Johansson, Epitaxial graphene on 6H-SiC and Li intercalation, *Phys. Rev. B* **82**, 205402 (2010).
- [33] S. Datta and B. Das, Electronic analog of the electro-optic modulator, *Appl. Phys. Lett.* **56**, 665 (1990).
- [34] E. R. Mucciolo, C. Chamon, and C. M. Marcus, Adiabatic Quantum Pump of Spin-Polarized Current, *Phys. Rev. Lett.* **89**, 146802 (2002).
- [35] M. Khodas, A. Shekhter, and A. M. Finkel'stein, Spin Polarization of Electrons by Nonmagnetic Heterostructures: The Basics of Spin Optics, *Phys. Rev. Lett.* **92**, 086602 (2004).
- [36] D. Bercioux and A. D. Martino, Spin-resolved scattering through spin-orbit nanostructures in graphene, *Phys. Rev. B* **81**, 165410 (2010).
- [37] D. Marchenko, A. Varykhalov, M. Scholz, G. Bihlmayer, E. Rashba, A. Rybkin, A. Shikin, and O. Rader, Giant Rashba splitting in graphene due to hybridization with gold, *Nat Commun* **3**, 1232 (2012).
- [38] M. M. Asmar and S. E. Ulloa, Rashba spin-orbit interaction and birefringent electron optics in graphene, *Phys. Rev. B* **87**, 075420 (2013).
- [39] W. Han, R. K. Kawakami, M. Gmitra, and J. Fabian, Graphene spintronics, *Nature Nanotech.* **9**, 794 (2014).
- [40] A. Avsar, H. Ochoa, F. Guinea, B. Özyilmaz, B. van Wees, and I. Vera-Marun, Colloquium : Spintronics in graphene and other two-dimensional materials, *Rev. Mod. Phys.* **92**, 021003 (2020).
- [41] Y. Nambu and G. Jona-Lasinio, Dynamical Model of Elementary Particles Based on an Analogy with Superconductivity. I, *Phys. Rev.* **122**, 345 (1961).
- [42] A. Obertelli and H. Sagawa, Modern Nuclear Physics (Springer Singapore, 2021), pp. 685–727.
- [43] C. W. J. Beenakker, N. V. Gnezdilov, E. Dresselhaus, V. P. Ostroukh, Y. Herasymenko, I. Adagideli, and J. Tworzydło, Valley switch in a graphene superlattice due to pseudo-Andreev reflection, *Phys. Rev. B* **97**, 241403 (2018).
- [44] M. I. Katsnelson, K. S. Novoselov, and A. K. Geim, Chiral tunnelling and the Klein paradox in graphene, *Nat. Phys.* **2**, 620 (2006).
- [45] P. E. Allain and J. N. Fuchs, Klein tunneling in graphene: optics with massless electrons, *Eur. Phys. J. B* **83**, 301 (2011).
- [46] R. Shen, L. B. Shao, B. Wang, and D. Y. Xing, Single Dirac cone with a flat band touching on line-centered-square optical lattices, *Phys. Rev. B* **81**, 041410 (2010).
- [47] D. F. Urban, D. Bercioux, M. Wimmer, and W. Häusler, Barrier transmission of Dirac-like pseudospin-one particles, *Phys. Rev. B* **84**, 115136 (2011).
- [48] H.-Y. Xu and Y.-C. Lai, Revival resonant scattering, perfect caustics, and isotropic transport of pseudospin-1 particles, *Phys. Rev. B* **94**, 165405 (2016).
- [49] Y. Betancur-Ocampo, G. Cordourier-Maruri, V. Gupta, and R. de Coss, Super-Klein tunneling of massive pseudospin-one particles, *Phys. Rev. B* **96**, 024304 (2017).
- [50] S. Nandy, K. Sengupta, and D. Sen, Transport across junctions of pseudospin-one fermions, *Phys. Rev. B* **100**, 085134 (2019).
- [51] S. Kim and K. Kim, Omnidirectional excitation of surface waves and super-Klein tunneling at the interface between two different bi-isotropic media, *Phys. Rev. B* **101**, 165428 (2020).
- [52] A. Contreras-Astorga, F. Correa, and V. Jakubský, Super-Klein tunneling of Dirac fermions through electrostatic gratings in graphene, *Phys. Rev. B* **102**, 115429 (2020).

- (2020).
- [53] H.-Y. Xu, L. Huang, and Y.-C. Lai, Klein scattering of spin-1 Dirac-Weyl wave and localized surface plasmon, *Phys. Rev. Research* **3**, 013284 (2021).
 - [54] C.-Z. Wang, H.-Y. Xu, and Y.-C. Lai, Super skew scattering in two-dimensional Dirac material systems with a flat band, *Phys. Rev. B* **103**, 195439 (2021).
 - [55] L. Mandhour and F. Bouhadida (2020), Klein tunneling in deformed $\alpha - T_3$ lattice, 2004.10144.
 - [56] Y. Betancur-Ocampo and V. Gupta, Perfect transmission of 3D massive Kane fermions in HgCdTe Veselago lenses, *J. Phys.: Condens. Matter* **30**, 035501 (2017).
 - [57] V. V. Cheianov and V. I. Fal'ko, Selective transmission of Dirac electrons and ballistic magnetoresistance of pn-junctions in graphene, *Phys. Rev. B* **74**, 041403 (2006).
 - [58] Y. Betancur-Ocampo, F. Leyvraz, and T. Stegmann, Electron Optics in Phosphorene pn Junctions: Negative Reflection and Anti-Super-Klein Tunneling, *Nano Lett.* **19**, 7760 (2019).
 - [59] E. Paredes-Rocha, Y. Betancur-Ocampo, N. Szpak, and T. Stegmann, Gradient-index electron optics in graphene p-n junctions, *Phys. Rev. B* **103**, 045404 (2021).